


## Uncovering the Mechanism of the Impurity-Selective Mott Transition in Paramagnetic $V_2O_3$

Frank Lechermann,<sup>1</sup> Noam Bernstein,<sup>2</sup> I. I. Mazin,<sup>2</sup> and Roser Valentí<sup>3</sup>

<sup>1</sup>*Institut für Theoretische Physik, Universität Hamburg, Jungiusstraße 9, D-20355 Hamburg, Germany*

<sup>2</sup>*Code 6393, Naval Research Laboratory, Washington, DC 20375, USA*

<sup>3</sup>*Institut für Theoretische Physik, Goethe-Universität Frankfurt, Max-von-Laue-Straße 1, 60438 Frankfurt am Main, Germany*

 (Received 26 January 2018; published 4 September 2018)

While the phase diagrams of the one- and multiorbital Hubbard model have been well studied, the physics of real Mott insulators is often much richer, material dependent, and poorly understood. In the prototype Mott insulator  $V_2O_3$ , chemical pressure was initially believed to explain why the paramagnetic-metal to antiferromagnetic-insulator transition temperature is lowered by Ti doping while Cr doping strengthens correlations, eventually rendering the high-temperature phase paramagnetic insulating. However, this scenario has been recently shown both experimentally and theoretically to be untenable. Based on full structural optimization, we demonstrate via the charge self-consistent combination of density functional theory and dynamical mean-field theory that changes in the  $V_2O_3$  phase diagram are driven by defect-induced local symmetry breakings resulting from dramatically different couplings of Cr and Ti dopants to the host system. This finding emphasizes the high sensitivity of the Mott metal-insulator transition to the local environment and the importance of accurately accounting for the one-electron Hamiltonian, since correlations crucially respond to it.

DOI: 10.1103/PhysRevLett.121.106401

**Introduction.**—After many decades of intense research, the  $V_2O_3$  phase diagram still stands out as a challenge in condensed matter physics [1–6]. Its canonical form (cf. Fig. 1) [7] has been addressed many times both experimentally and theoretically. At stoichiometry and at ambient temperature  $T$ , a paramagnetic-metallic (PM) phase in a corundum crystal structure is stable. Driving the temperature below  $T_N \sim 155$  K results in an antiferromagnetic-insulating (AFI) phase with a monoclinic crystal structure. Ti doping rapidly suppresses this low- $T$  phase, whereas Cr doping stabilizes it, and, additionally, transforms the high- $T$  PM phase into a paramagnetic-insulating (PI) one.

$V^{3+}$  has two  $3d$  electrons, occupying the triply degenerate (for each spin)  $t_{2g} = \{e_g^\pi, a_{1g}\}$  orbitals, split into a lower  $e_g^\pi$  doublet and an upper  $a_{1g}$  singlet in the trigonal crystal field (CF) of the corundum structure. In the low- $T$  monoclinic structure, the additional low-symmetry CF component lifts the  $e_g^\pi$  degeneracy. At first glance, the experimental phase diagram shown in Fig. 1 seems consistent with a positive (negative) chemical pressure exerted by Ti (Cr) doping. It has, therefore, been routinely interpreted in terms of the standard picture derived from the Hubbard model: upon applying positive (negative) pressure, the bandwidth  $W$  increases (decreases), and so does the ratio  $W/U$ , which controls the correlation strength and thus the tendency to form a metal. This picture has been accepted in many previous works and appeared to be supported [4,8–10] by

a combination of density functional theory (DFT) and dynamical mean-field theory (DMFT) without charge self-consistency (i.e., one-shot scheme), whereupon the correlation-enhanced CF splitting leads to a strong orbital polarization towards  $e_g^\pi$  already at stoichiometry. However, by finding still sizable  $a_{1g}$  filling at zero doping, this scenario

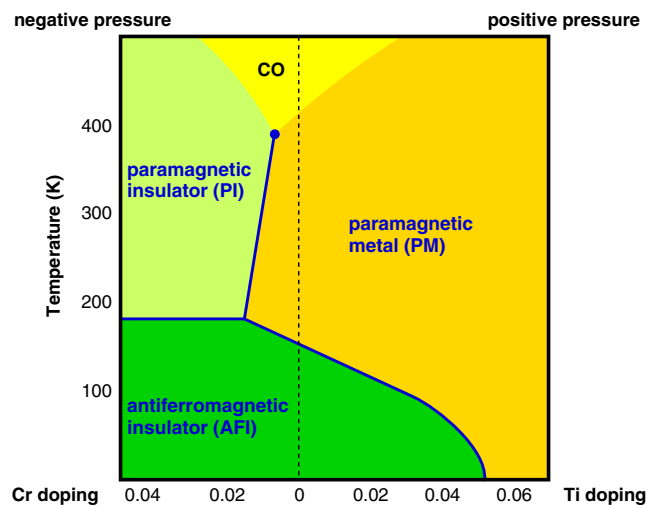


FIG. 1.  $V_2O_3$  phase diagram (after [7]), with “CO” marking the crossover region. Note that the doping axis indicates the *effect* on the phase boundary similar to pressure, but not necessarily the corresponding volume change or mechanism.

has recently been questioned by angle-resolved photoemission [11] and charge self-consistent DFT + DMFT calculations [12–15]. The chemical-pressure effect is apparently too weak to explain key  $V_2O_3$  phenomenology. In addition, contrary to many statements in the literature, Ti doping leads to a volume *increase* [16], although less so than Cr.

Alternative causes for this metal-insulator transition (MIT) were postulated [2,17–23]. Early on, Rice and Brinkman [17] blamed doping-induced disorder and scattering for the metallicity breakdown. Indeed, ion-irradiation experiments revealed the sensitivity of the transition temperature to even a small concentration of defects [24]. However, while such a scenario could explain why Cr doping leads to an insulating state, it fails to explain the opposite effect of Ti doping.

In this Letter, we show that the key effects of Cr or Ti doping cannot be reduced to a chemical pressure. Instead, in a first approximation, the Cr effect (reduced metallicity) is mostly structural (reduced local symmetry around Cr ion). The opposite effect of Ti is mostly electronic, an effective electron (and not hole) doping of  $V_2O_3$ . This conclusion is based upon a first-principles study employing state-of-the-art charge-self-consistent DFT + DMFT calculations on relaxed supercells with Cr or Ti doping. We emphasize that both a proper account of the structural and charge self-consistency effects on the realistic defect chemistry, as well as a precise inclusion of correlation effects, are essential for describing the physics of  $V_2O_3$ .

*Structural aspects.*—The starting point for the DFT + DMFT calculations is the canonical two-formula unit cell at stoichiometry (below called the “stoichiometric” case), reported in Ref. [25]. We first address the *global* structural effects of doping (chemical pressure) by considering the minimal unit cell as reported by the experiment, i.e., averaged over the impurity disorder, for 2.8% Cr [25] and 3% Ti [16] doping (“experimental-averaged” Cr or Ti, EA-Cr and EA-Ti, respectively). For both dopings, the *c*-axis (*a*-axis) parameter is reduced (increased) and the resulting volumes are larger than at stoichiometry. However, the so-called “umbrella” distortion, i.e., the disparity of the two sets of O-metal-O angles, changes only marginally in EA-Ti (from  $15.8^\circ$  to  $16.1^\circ$ ), but increases noticeably to  $18.5^\circ$  with Cr.

Next, we construct 80-atom  $2 \times 2 \times 2$  supercells with one of the 32 V sites replaced by Cr or Ti, i.e., a 3.1% doping, with the cell dimensions of the EA structures, and applied full symmetry-unrestricted atomic relaxation with density functional theory with the Hubbard  $U$  parameter (DFT +  $U$ ). Upon structural relaxation, the V ions near Cr shift toward the impurity, whereas the V-V distance of V ions farther away from the dopant increases, both in line with experiment [21,22]. For Ti doping, on the other hand, V ions are repelled from the impurity. Second, local monoclinic distortions are favored in Cr-doped  $V_2O_3$ , in agreement with experiment [18,20,22], but not in the Ti-doped compound. Note that due to the limitations in manageable supercell sizes, the local monoclinic distortions are described by a complete

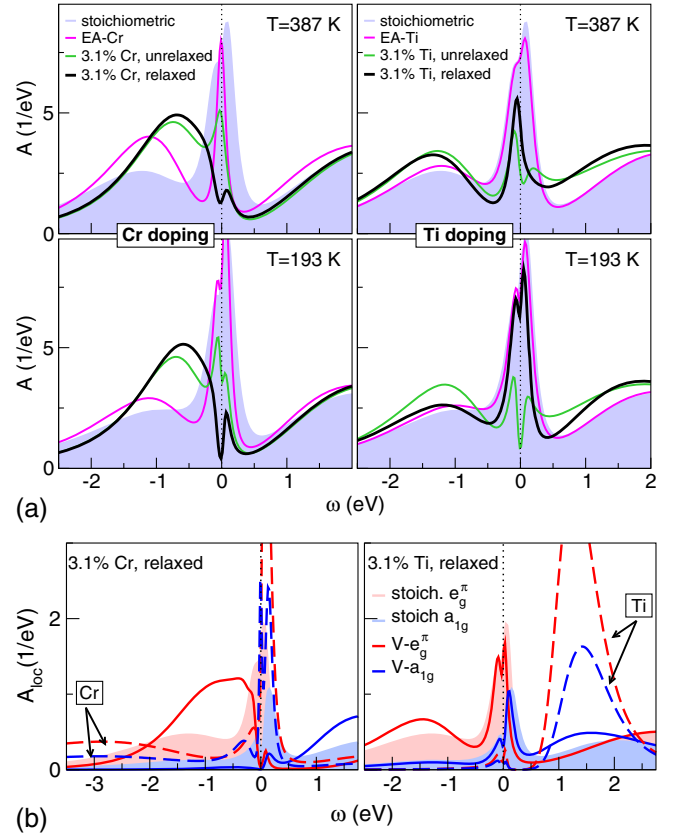


FIG. 2. DFT + DMFT spectral functions of stoichiometric and doped  $V_2O_3$ . (a) Total spectral function at two  $T$  for Cr doping (left) and Ti doping (right). (b) Lattice-averaged  $V-e_g^\pi$  and  $V-a_{1g}$  (full lines), and Cr and Ti  $e_g^\pi$  and  $a_{1g}$  (dashed lines) local spectral function at  $T = 193$  K, compared to orbital-resolved stoichiometric  $A_{loc}$  (shaded areas).

symmetry change of the defect cell. Nevertheless, starting from the experimental corundum structure, fixing the lattice parameters, and using a local-minimum relaxation algorithm ensures that the resulting structure is a good approximation of the true defect geometry. More details of the structural optimization are provided in the Supplemental Material [26].

A charge self-consistent DFT + DMFT scheme [12, 32,33] is applied to thus obtained structures. The  $V-t_{2g}$  triplet defines the correlated subspace, with a Hubbard  $U = 5$  eV and Hund’s-rule coupling  $J_H = 0.7$  eV (for more details see Supplemental Material with Refs. [34–39]).

Figure 2 shows the calculated spectral functions at  $T = 387$  K and  $T = 193$  K. Stoichiometric  $V_2O_3$  [Fig. 2(a) shaded region] displays a bare trigonal CF splitting of 162 meV. A moderate orbital polarization towards  $e_g^\pi$  is seen from the values of  $n \equiv \{n_{e_g^\pi}, n_{a_{1g}}\} = \{1.58, 0.42\}$ . It is a correlated metal with a renormalized quasiparticle (QP) peak and Hubbard bands, in line with photoemission observations [6,40]. Based on the spectral weight of the lower Hubbard band, the correlation strength appears to be somewhat larger at *higher*  $T$ . This is due to the

small orbital-dependent coherence-energy scale in  $V_2O_3$  [10,26,41]; when the temperature hits this scale, the low-energy QPs start to lose coherence and spectral-weight transfer to the Hubbard sidebands occurs.

*Ti doping.*—First, we investigate Ti doping with the various unit cells and supercells described above (Fig. 2, right panels). The effective EA-Ti case remains clearly metallic. Without structural relaxation, the supercell case opens a pseudogap due to a Kondo-insulator-like hybridization between the V bands and Ti impurity states. Upon relaxations, Ti- $t_{2g}$  states shift up, the artificial hybridization vanishes, and the system becomes strongly metallic. Since the Ti- $t_{2g}$  states [Fig. 2(b)] are higher than V ones, Ti loses all electrons and dopes the V bands;  $(V_{1-x}Ti_x)_2O_3$  is thus electronically equivalent to  $V_2O_3$  doped with  $x/(1-x)$  electrons. At low temperatures, as any doped Mott insulator, the system rapidly metallizes [Fig. 2(a) right panels]. This is also clearly seen in the DFT +  $U$  calculations (cf. Fig. 5). The formal valence of the Ti impurity is now 4+, in agreement with experiment [42]. Note that  $Ti^{4+}$  has a smaller ionic radius (74.5 pm [43]) than the  $V^{3+}$  one (78 pm) causing a *positive* chemical pressure, opposite to what would have happened for  $Ti^{3+}$  (81 pm).

*Cr doping.*—This case is more complex and Fig. 2 shows our main results. Pure  $V_2O_3$  set in the EA-Cr structure does not exhibit a tendency to gap formation [pink curves in Fig. 2(a)], contrary to earlier one-shot DFT + DMFT calculations [10]. The orbital polarization towards  $e_g^\pi$  remains moderate (see the Supplemental Material [26] for a complete account of the respective orbital occupations and a further analysis with Refs. [44–46]), unless unrealistically large lattice expansion is assumed [12,15]. However, a complete structural relaxation with impurity-induced local monoclinic distortions leads to a gap opening in the paramagnetic phase as shown by the disappearance of spectral weight at low energy (3.1% Cr, relaxed, black curves). The gap size of  $\sim 100$  meV (at  $T = 193$  K) is in excellent agreement with experiment [40,47]. While even the simple replacement of a single V ion by Cr already leads to a reduction of low-energy spectral weight and strengthening of correlations [13] (3.1% Cr, unrelaxed, green curves), structural relaxation is required for opening the gap. From analyzing the local spectral functions we find a complete MIT, i.e., no sign of orbital-selective behavior [9,15] as shown in Fig. 2(b), where the lattice-averaged V- $e_g^\pi$  and V- $a_{1g}$  function for the 3.1% Cr, relaxed structure (solid line) is plotted. Figure 3 shows that under external pressure the PI phase recovers metallicity, in agreement with experimental work by Rodolakis *et al.* [48]. Importantly, this stabilized metallic phase is not identical to the original stoichiometric one. Instead, it shows a sizable pseudogap and a large part of the Cr-induced  $e_g^\pi$  polarization is preserved. For comparison, the experimental low- $T$  monoclinic structure at stoichiometry [49] is easily Mott insulating already in paramagnetic DFT + DMFT

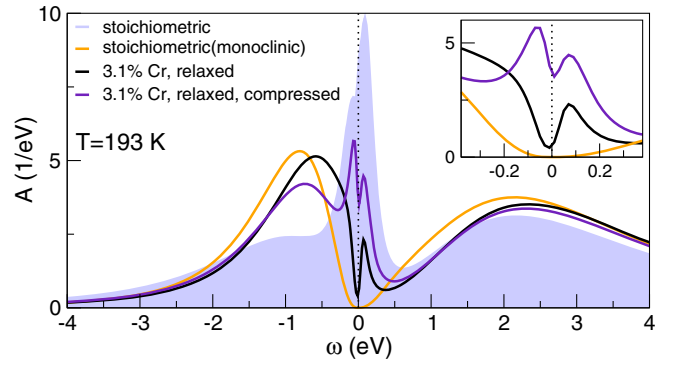


FIG. 3. DFT + DMFT spectral functions at stoichiometry and with 3.1% Cr doping. Compressed Cr-doped case: relaxed supercell structure with stoichiometric lattice parameters. Stoichiometric (monoclinic) case: experimental low- $T$  monoclinic structure without doping, here at  $T = 193$  K treated as paramagnetic, with a monoclinic bare CF splitting  $\Delta e_g^\pi = 29$  meV and an orbital filling  $n = \{1.96, 0.04\}$ . Inset: low-energy enlargement.

(see Fig. 3, orange line), with a sizable charge gap of about 0.4 eV.

Obviously, Cr behaves completely differently with respect to the V matrix of  $V_2O_3$  compared to Ti. This can be traced to several effects. First, the one-electron Cr- $t_{2g}$  level is *below* the entire V- $t_{2g}$  manifold (as shown from DFT +  $U$  calculations in the Supplemental Material [26]), and reflected in a broad impurity state centered at  $-2.8$  eV in Fig. 2(b) (which is reminiscent of a similar feature around  $-2$  eV in photoemission [40]). Formally, the  $Cr^{3+}$  ion as three valence electrons, which constitute a spin  $S = 3/2$  state below the V- $t_{2g}$  states. The formal occupancy of the V- $e_g^\pi$  states remains essentially unaltered, so one has to look at more subtle, structural effects. First, the  $Cr^{3+}$  ionic radius [43] of 75.5 pm indeed causes positive chemical pressure. Second, the stronger and more asymmetric trigonal distortion (“umbrella distortion,” UD) of the EA-Cr structure, compared to stoichiometric  $V_2O_3$ , creates a stronger  $e_g^\pi$ - $a_{1g}$  splitting. With the Cr impurity but without any further structural changes, the orbital polarization towards  $e_g^\pi$  is then already very strong with  $n = \{1.87, 0.10\}$ . Yet only the additional monoclinic CF triggered by the explicit local-symmetry breaking effects of Cr doping finally drives the MIT. Note that this additional CF splitting is only  $\Delta e_g^\pi \sim 5$ –20 meV, depending on the V site, but it proves relevant to establishing the PI phase. Multiorbital Mott transitions driven by subtle CF splitting have been studied in various model-Hamiltonian schemes [50,51].

However, importantly, the Cr-induced UD plays its own, quite essential role, albeit indirectly. In order to address the effect of the structure symmetry alone, we have performed calculations using the high-symmetry EA-Cr, stoichiometric and EA-Ti structures (which differ mostly by the degree of the UD), and artificially lowered the symmetry by randomly

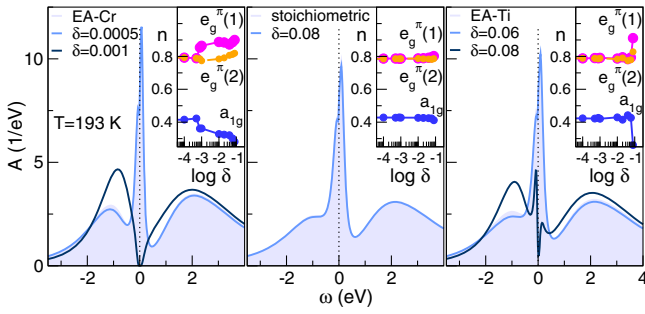


FIG. 4. DFT + DMFT data for the small unit cells EA-Cr (left), stoichiometric (middle), and EA-Ti (right) with symmetry-breaking charge-density modifications: selected total spectral functions and orbital occupations (inset). The quantity  $\delta$  marks the O-nuclei charge deviation on site  $i$ , i.e.,  $Z_i(\tilde{O}) = Z_i(O) + \delta_i$  for distributed  $\delta_i = (-1)^i \delta$  with  $\sum_{\text{cell}} \delta_i = 0$  [26].

replacing the ligand oxygens with pseudo-oxygen of nuclear (and electron) charge  $8 \pm \delta$  (see the Supplemental Material [26] for more details). The result of this experiment is shown in Fig. 4. While EA-Cr transforms into a Mott insulator at an already tiny symmetry-lowering field, the other metallic structures remain comparatively robust to such a field. Thus, the same high-symmetry corundum structure is much more sensitive to symmetry lowering if it has a stronger UD asymmetry, as is the case in EA-Cr.

This effect is the leading source of the insulating behavior in Cr-doped samples, but is by far not the only effect present. For instance, charge fluctuations and Kondo-like screening of the additional Cr spin generate an empty QP peak [dashed curve in Fig. 2(b), left panel] just at the bottom of the upper gap edge, which can, in principle, be visible in inverse photoemission. Notably, this feature should lead to a *decrease* of the charge gap at low temperatures with Cr doping. And indeed, this originally counterintuitive gap development is observed in photoemission [40].

**DFT +  $U$  calculations.**—We have established above that the charge self-consistent DFT + DMFT supercell calculations, which include local correlation effects, are capable of reproducing the experimental trends for both kinds of doping (Cr and Ti) when distortions around impurities and charge alteration are accounted for. At this point, it is instructive to ask which effects introduced by doping are already captured by an effective one-electron approach. To this end, we analyze here whether the static mean-field DFT +  $U$  method shows the right trends of increasing (reducing) the low- $T$  gap when doping  $V_2O_3$  by Cr (Ti). We use DFT +  $U$  with  $U_{\text{eff}} = U - J = 1.5$  eV to relax (with respect to atomic position and cell shape, but not volume) our minimal two-formula unit cells at the experimental Cr and Ti doped volumes. Additionally, our already relaxed 80-atom supercells with impurities are further optimized with that protocol in order to realize now the low- $T$  scenario. For all these structures, the band gap as a function of  $U_{\text{eff}}$  is computed (Fig. 5). When optimized at the volume

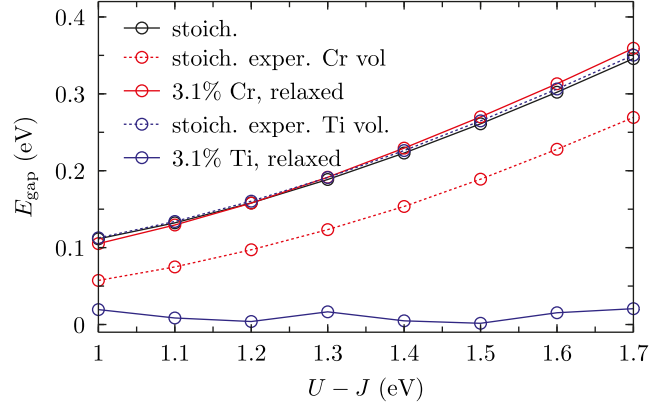


FIG. 5. DFT +  $U$  band gap as a function of  $U_{\text{eff}}$  for the pure stoichiometric system, the pure system at volumes equivalent to the experimental 2.8% Cr and 3% Ti doped volumes, and supercells with one atom of V substituted by Cr and Ti.

of the experimental Ti-doped material, the undoped system has essentially the same gap as at the pure material volume, while at the experimental Cr-doped volume the gap goes *down* by about 0.07 eV. However, the same procedure applied to the relaxed supercells of the doped systems leads to a completely different behavior: for Ti doping the gap is reduced to zero (within computational noise), while for Cr doping the gap increases slightly over the original pure material's band gap. We should point out that, for the purpose of uniformity, we have used the same optimization procedure for all compound scenarios. While a much larger  $U_{\text{eff}}$  is needed to open a gap in the high- $T$  corundum structure, in the optimized low-symmetry  $T = 0$  AF structure the gap opens already at  $U - J \lesssim 1$  eV. These results demonstrate that the opposite, and qualitatively correct, trends of Cr vs Ti doping are captured at the effective one-electron level. However, correlation effects as implemented in DMFT are essential to describe the PM-PI transition at finite temperatures and distinguish between the less correlated undoped behavior and the more correlated Cr-doped case.

**Conclusions.**—Our charge self-consistent results prove that the intriguing Cr- and Ti-doping phase diagram of  $V_2O_3$  is not driven by chemical pressure. In fact, contrary to the common misconception, the principal factors controlling the phase diagram are qualitatively different for the two impurities. On the Cr side, the main factor is a local structural distortion affecting the crystal field, while on the Ti side it is effective electron doping by virtue of Ti acquiring a valence of 4+. Increasing the umbrella distortion in the average corundum structure by Cr doping is not *per se* sufficient to trigger a paramagnetic insulator, but it makes the system more sensitive to further symmetry lowering on the local level. In the simplest approximation, Ti produces a charge doping and Cr does not, while Cr produces a structural distortion conducive to insulating behavior and Ti does not.

Our findings elucidate the major factors controlling the phase diagram of vanadium sesquioxide, and should also be relevant to interpret recent  $V_2O_3$  thin-film studies [52,53]. We, furthermore, observe that whereas these effects are importantly enhanced by electron correlations, the described trends appear already at the one-electron level within the static mean-field DFT +  $U$  framework.

We thank J. W. Allen, J. D. Denlinger, and I. K. Schuller for helpful discussions. F. L. acknowledges financial support from the DFG Project No. LE 2446/4-1. I. I. M. and N. B. were supported by Office of Naval Research (ONR) through the Naval Research Laboratory (NRL) basic research program. R. V. was supported by the DFG through SFB/TR 49. DFT + DMFT computations were performed at the JURECA Cluster of the Jülich Supercomputing Centre (JSC) under Project No. hhh08.

- 
- [1] T. M. Rice and D. B. McWhan, *IBM J. Res. Dev.* **14**, 251 (1970).
- [2] C. Castellani, C. R. Natoli, and J. Ranninger, *Phys. Rev. B* **18**, 4945 (1978).
- [3] J.-H. Park, L. H. Tjeng, A. Tanaka, J. W. Allen, C. T. Chen, P. Metcalf, J. M. Honig, F. M. F. de Groot, and G. A. Sawatzky, *Phys. Rev. B* **61**, 11506 (2000).
- [4] K. Held, G. Keller, V. Eyert, D. Vollhardt, and V. I. Anisimov, *Phys. Rev. Lett.* **86**, 5345 (2001).
- [5] T. Saha-Dasgupta, O. K. Andersen, J. Nuss, A. I. Poteryaev, A. Georges, and A. I. Lichtenstein, *arXiv:0907.2841*.
- [6] H. Fujiwara, A. Sekiyama, S.-K. Mo, J. W. Allen, J. Yamaguchi, G. Funabashi, S. Imada, P. Metcalf, A. Higashiya, and M. Yabashi *et al.*, *Phys. Rev. B* **84**, 075117 (2011).
- [7] D. B. McWhan, T. M. Rice, and J. B. Remeika, *Phys. Rev. Lett.* **23**, 1384 (1969); D. B. McWhan, J. B. Remeika, T. M. Rice, W. F. Brinkman, J. P. Maita, and A. Menth, *Phys. Rev. Lett.* **27**, 941 (1971); D. B. McWhan, A. Menth, J. B. Remeika, T. M. Rice, and W. F. Brinkman, *Phys. Rev. B* **7**, 1920 (1973).
- [8] G. Keller, K. Held, V. Eyert, D. Vollhardt, and V. I. Anisimov, *Phys. Rev. B* **70**, 205116 (2004).
- [9] M. S. Laad, L. Craco, and E. Müller-Hartmann, *Phys. Rev. B* **73**, 045109 (2006).
- [10] A. I. Poteryaev, J. M. Tomczak, S. Biermann, A. Georges, A. I. Lichtenstein, A. N. Rubtsov, T. Saha-Dasgupta, and O. K. Andersen, *Phys. Rev. B* **76**, 085127 (2007).
- [11] I. Lo Vecchio, J. D. Denlinger, O. Krupin, B. J. Kim, P. A. Metcalf, S. Lupi, J. W. Allen, and A. Lanzara, *Phys. Rev. Lett.* **117**, 166401 (2016).
- [12] D. Grieger, C. Piefke, O. E. Peil, and F. Lechermann, *Phys. Rev. B* **86**, 155121 (2012).
- [13] D. Grieger and F. Lechermann, *Phys. Rev. B* **90**, 115115 (2014).
- [14] X. Deng, A. Sternbach, K. Haule, D. N. Basov, and G. Kotliar, *Phys. Rev. Lett.* **113**, 246404 (2014).
- [15] I. Leonov, V. I. Anisimov, and D. Vollhardt, *Phys. Rev. B* **91**, 195115 (2015).
- [16] S. Chen, J. E. Hahn, C. E. Rice, and W. R. Robinson, *J. Solid State Chem.* **44**, 192 (1982).
- [17] T. M. Rice and W. F. Brinkman, *Phys. Rev. B* **5**, 4350 (1972).
- [18] P. Pfalzer, J. Will, A. Nateprov, Jr., M. Klemm, V. Eyert, S. Horn, A. I. Frenkel, S. Calvin, and M. L. denBoer, *Phys. Rev. B* **66**, 085119 (2002).
- [19] A. Tanaka, *J. Phys. Soc. Jpn.* **71**, 1091 (2002).
- [20] A. Bombardi, F. de Bergevin, S. D. Matteo, L. Paolasini, P. A. Metcalf, and J. M. Honig, *Physica (Amsterdam)* **345B**, 40 (2004).
- [21] A. I. Frenkel, D. M. Pease, J. I. Budnick, P. Metcalf, E. A. Stern, P. Shanthakumar, and T. Huang, *Phys. Rev. Lett.* **97**, 195502 (2006).
- [22] C. Meneghini, S. Di Matteo, C. Monesi, T. Neisius, L. Paolasini, S. Mobilio, C. R. Natoli, P. A. Metcalf, and J. M. Honig, *J. Phys. Condens. Matter* **21**, 355401 (2009).
- [23] Y. Guo, S. J. Clark, and J. Robertson, *J. Chem. Phys.* **140**, 054702 (2014).
- [24] J. G. Ramirez, T. Saerbeck, S. Wang, J. Trastoy, M. Malnou, J. Lesueur, J.-P. Crocombette, J. E. Villegas, and I. K. Schuller, *Phys. Rev. B* **91**, 205123 (2015).
- [25] P. D. Dernier, *J. Phys. Chem. Solids* **31**, 2569 (1970).
- [26] See Supplemental Material at <http://link.aps.org/supplemental/10.1103/PhysRevLett.121.106401> for details on the electronic structure calculations and the structural optimization. Furthermore, it includes a DFT account of the Cr-doped case, density of states and energy levels from DFT +  $U$ , as well as orbital occupations, k-resolved spectral functions and a view on temperature effects from DFT + DMFT, which including Refs. [27–31].
- [27] G. Kresse and J. Furthmüller, *Phys. Rev. B* **54**, 11169 (1996).
- [28] J. P. Perdew, K. Burke, and M. Ernzerhof, *Phys. Rev. Lett.* **77**, 3865 (1996).
- [29] V. I. Anisimov, I. V. Solovyev, M. A. Korotin, M. T. Czyżyk, and G. A. Sawatzky, *Phys. Rev. B* **48**, 16929 (1993).
- [30] S. G. Louie, K. M. Ho, and M. L. Cohen, *Phys. Rev. B* **19**, 1774 (1979).
- [31] B. Meyer, C. Elsässer, F. Lechermann, and M. Fähnle, fortran 90 program for mixed-basis-pseudopotential calculations for crystals.
- [32] S. Y. Savrasov, G. Kotliar, and E. Abrahams, *Nature (London)* **410**, 793 (2001).
- [33] L. V. Pourovskii, B. Amadon, S. Biermann, and A. Georges, *Phys. Rev. B* **76**, 235101 (2007).
- [34] B. Amadon, F. Lechermann, A. Georges, F. Jollet, T. O. Wehling, and A. I. Lichtenstein, *Phys. Rev. B* **77**, 205112 (2008).
- [35] V. I. Anisimov, D. E. Kondakov, A. V. Kozhevnikov, I. A. Nekrasov, Z. V. Pchelkina, J. W. Allen, S.-K. Mo, H.-D. Kim, P. Metcalf, S. Suga *et al.*, *Phys. Rev. B* **71**, 125119 (2005).
- [36] A. N. Rubtsov, V. V. Savkin, and A. I. Lichtenstein, *Phys. Rev. B* **72**, 035122 (2005).
- [37] P. Werner, A. Comanac, L. de’ Medici, M. Troyer, and A. J. Millis, *Phys. Rev. Lett.* **97**, 076405 (2006).

- [38] O. Parcollet, M. Ferrero, T. Ayrat, H. Hafermann, I. Krivenko, L. Messio, and P. Seth, *Comput. Phys. Commun.* **196**, 398 (2015).
- [39] P. Seth, I. Krivenko, M. Ferrero, and O. Parcollet, *Comput. Phys. Commun.* **200**, 274 (2016).
- [40] S.-K. Mo, H.-D. Kim, J. D. Denlinger, J. W. Allen, J.-H. Park, A. Sekiyama, A. Yamasaki, S. Suga, Y. Saitoh, T. Muro *et al.*, *Phys. Rev. B* **74**, 165101 (2006).
- [41] I. Lo Vecchio, L. Baldassarre, P. Di Pietro, F. Giorgianni, M. Marsi, A. Perucchi, U. Schade, A. Lanzara, and S. Lupi, *J. Phys. Condens. Matter* **29**, 345602 (2017).
- [42] S.-K. Mo, Ph.D. thesis, University of Michigan, 2006.
- [43] R. D. Shannon, *Acta Crystallogr. Sect. A* **A32**, 751 (1976).
- [44] V. Eyert, *Ann. Phys. (Berlin)* **11**, 650 (2002).
- [45] F. Cyrot-Lackmann, *J. Phys. Chem. Solids* **29**, 1235 (1968).
- [46] A. P. Sutton, *Electronic Structure of Materials* (Oxford University Press, Oxford, 1993).
- [47] A. S. Barker, Jr. and J. P. Remeika, *Solid State Commun.* **8**, 1521 (1970).
- [48] F. Rodolakis, P. Hansmann, J.-P. Rueff, A. Toschi, M. W. Haverkort, G. Sangiovanni, A. Tanaka, T. Saha-Dasgupta, O. K. Andersen, K. Held *et al.*, *Phys. Rev. Lett.* **104**, 047401 (2010).
- [49] P. D. Dernier and M. Marezio, *Phys. Rev. B* **2**, 3771 (1970).
- [50] N. Manini, G. E. Santoro, A. Dal Corso, and E. Tosatti, *Phys. Rev. B* **66**, 115107 (2002).
- [51] T. Kita, T. Ohashi, and N. Kawakami, *Phys. Rev. B* **84**, 195130 (2011).
- [52] S. S. Majid, D. K. Shukla, F. Rahman, K. Gautam, R. J. Choudhary, V. G. Sathe, and D. M. Phase, *Appl. Phys. Lett.* **110**, 173101 (2017).
- [53] E. B. Thorsteinsson, S. Shayestehaminzadeh, and U. B. Arnalds, *Appl. Phys. Lett.* **112**, 161902 (2018).